



Contents lists available at ScienceDirect

Bioorganic & Medicinal Chemistry Letters

journal homepage: www.elsevier.com/locate/bmcl

Diazinones as P2 replacements for pyrazole-based cathepsin S inhibitors

Michael K. Ameriks^{a,*}, Scott D. Bembenek^a, Matthew T. Burdett^b, Ingrid C. Choong^b, James P. Edwards^a, Damara Gebauer^{a,†}, Yin Gu^{a,†}, Lars Karlsson^a, Hans E. Purkey^b, Bart L. Staker^c, Siquan Sun^a, Robin L. Thurmond^a, Jian Zhu^a

^a Johnson & Johnson Pharmaceutical Research & Development, L.L.C., 3210 Merryfield Row, San Diego, CA 92121, USA

^b Sunesis Pharmaceuticals, 341 Oyster Point Boulevard, South San Francisco, CA 94080, USA

^c deCODE Biostructures, Inc., 7869 Northeast Day Road West, Bainbridge Island, WA 98110, USA

ARTICLE INFO

Article history:

Received 1 May 2010

Accepted 20 May 2010

Available online 25 May 2010

Keywords:

Cathepsin

Protease

Tethering

X-ray crystallography

Fragment-based screening

ABSTRACT

A pyridazin-4-one fragment **4** (hCatS IC₅₀ = 170 μM) discovered through Tethering was modeled into cathepsin S and predicted to overlap in S2 with the tetrahydropyridinepyrazole core of a previously disclosed series of CatS inhibitors. This fragment served as a template to design pyridazin-3-one **12** (hCatS IC₅₀ = 430 nM), which also incorporates P3 and P5 binding elements. A crystal structure of **12** bound to Cys25Ser CatS led to the synthesis of the potent diazinone isomers **22** (hCatS IC₅₀ = 60 nM) and **27** (hCatS IC₅₀ = 40 nM).

© 2010 Elsevier Ltd. All rights reserved.

The cathepsins comprise a large group of proteases whose general function involves protein degradation, processing, and turnover.¹ Cathepsin S (CatS), a cysteine protease of the papain family, resides in the lysosome of certain antigen-presenting cells and plays a key role in facilitating antigen presentation to CD4⁺ T-cells.² CatS-deficient mice exhibit defects in antigen processing, as well as a reduced susceptibility to collagen-induced arthritis compared to wild-type animals.³ Recently, additional pharmacologically relevant activities have also been attributed to CatS.⁴ We have previously reported a series of non-covalent CatS inhibitors with a tetrahydropyridinepyrazole core.⁵ This scaffold was originally discovered through a high-throughput screening (HTS) campaign and further optimized to provide compounds such as **1**⁶ and **2**⁷ (Fig. 1).

As a complementary approach to the traditional HTS strategy for lead generation, we also envisioned using fragment-based screening protocols to identify low molecular weight CatS inhibitors.⁸ Since proteases possess numerous extended binding sites in which each amino acid of the peptide or protein substrate occupies its own subsite, it was anticipated that cathepsin S would be an ideal target for fragment-based drug discovery.⁹ To this end, we employed a technique known as Tethering,¹⁰ in which site-directed mutagenesis was used to introduce cysteine residues into

various subsites of a Cys25Ser mutant form of CatS.¹¹ Each individual construct was then screened against a library of disulfide-containing compounds under reducing conditions, and the resulting fragments that formed stable protein–ligand disulfide adducts were characterized by mass spectrometry. In this letter, we describe how a low-affinity pyridazinone fragment **4** (Fig. 2) discovered through naïve Tethering was optimized for binding in S2 and linked to P3 and P5 groups previously identified for a

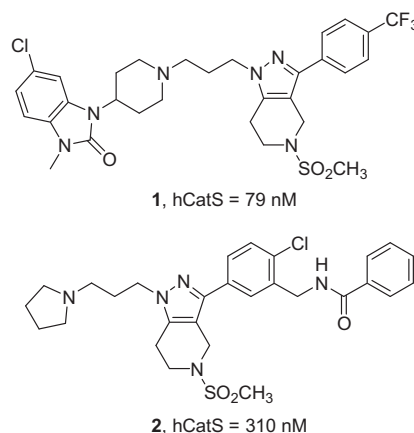


Figure 1. Representative pyrazole-based cathepsin S inhibitors.

* Corresponding author.

E-mail address: mameriks@its.jnj.com (M.K. Ameriks).

† Former employee of Johnson & Johnson Pharmaceutical Research & Development, L.L.C., 3210 Merryfield Row, San Diego, CA 92121, USA.

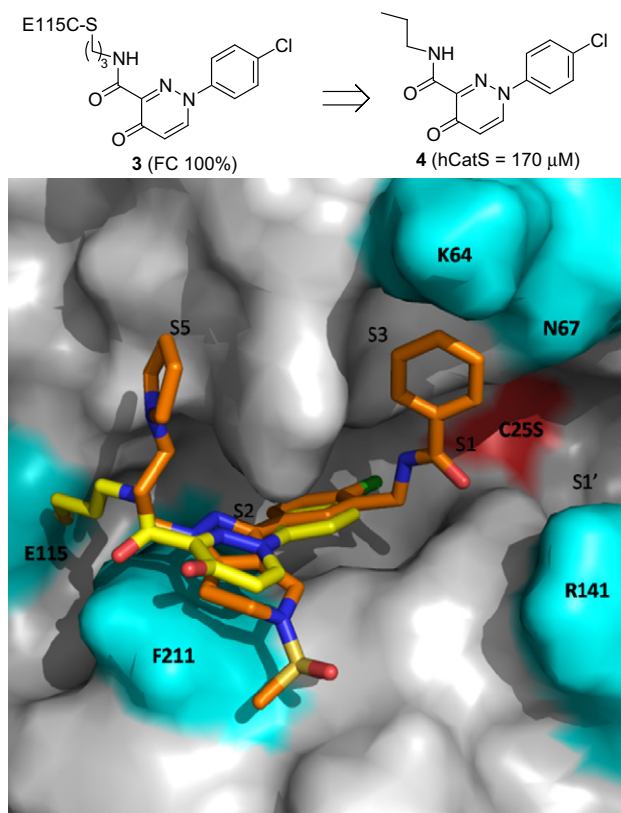


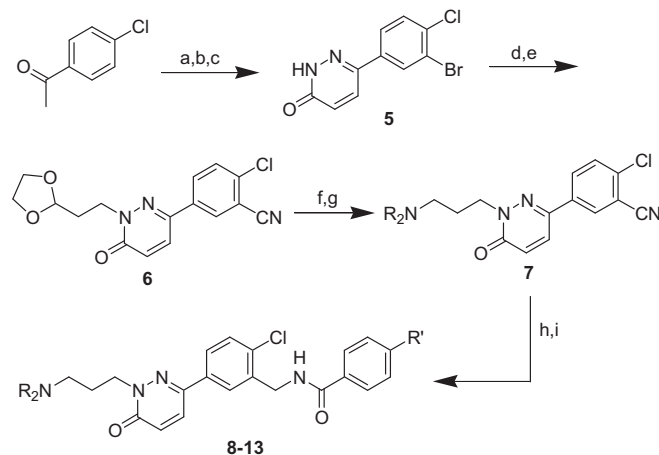
Figure 2. Docking model of Tethering hit **3** (yellow) overlaid with crystal structure of pyrazole-based CatS inhibitor **2** (orange). The residues at which cysteine mutations were introduced individually to enable Tethering are shown in cyan.

tetrahydropyridinepyrazole P2 core to provide a new series of potent diazinone-based CatS inhibitors.

In order to ensure adequate spatial coverage of the cathepsin S topography, five individual mutant constructs of Cys25Ser cathepsin S were prepared for Tethering: Lys64Cys, Asn67Cys, Glu115Cys, Phe211Cys, and Arg141Cys (Fig. 2).¹² Approximately 16,500 compounds from the Sunesis disulfide monophore library were screened against each construct, and 352 monophores exhibited >50% fractional conjugation (monophore-labeled CatS/total CatS) with any of the proteins.¹³ Roughly a third of these hits bound to the Glu115Cys mutant, including pyridazinone **3**, which completely labeled the protein (100% fractional conjugation at 1 mM β -ME). To confirm the viability of using this Tethering hit for subsequent lead optimization, the corresponding des-sulfide monophore fragment **4** was assayed against wild-type CatS (hCatS IC_{50} = 170 μ M).¹⁴

Although a X-ray crystal structure of the disulfide protein–ligand adduct **3** could not be obtained, the binding mode from our docking model suggested that the pyridazinone fragment resides in the S2 pocket of CatS (Fig. 2).¹⁵ Furthermore, when **3** was modeled into a Cys25Ser CatS cocrystal structure of pyrazole-based inhibitor **2**, several key features overlapped between the two structures: (1) the 4-chlorophenyl rings in S2, (2) the nitrogen atoms at N2 of the pyridazinone and pyrazole rings, and (3) the dihedral angles between the 4-chlorophenyl ring and the attached heterocyclic S2 cores (ϕ = 29° for pyridazinone **3** and 36° for pyrazole **2**). Notably, the Tethering hit lacks the P3 amide and P5 pyrrolidine groups found in pyrazole **2**. Thus, despite the low affinity of fragment **4** for CatS, it seemed possible that incorporating these additional binding elements would provide an opportunity to ‘grow’ the fragment into a potent CatS inhibitor.

Rather than preparing direct analogs of pyridazin-4-one **4**, we initially focused on the regioisomeric pyridazin-3-ones (**8–13**, Scheme 1) for two reasons: it was anticipated that this heterocycle would provide better overlap with both ring nitrogens in the pyrazole core, and the synthetic route to this class of compounds was well precedented.¹⁶ Thus, 6-arylpyridazin-3-one **6** was prepared in five steps from 4'-chloroacetophenone. This functionalized intermediate allowed for late-stage incorporation of the P3 and P5 groups. The P5 amines could be installed via a two-step procedure involving acetal hydrolysis and reductive amination, followed by nitrile reduction and acylation to introduce the P3 amide. During the optimization of this synthetic sequence, we observed that Raney-Ni was the only reducing agent capable of cleanly converting



Scheme 1. Reagents and conditions: (a) $AlCl_3$, Br_2 , DCE, rt (85%); (b) glyoxylic acid, 120 °C; (c) H_2NNH_2 , aq NH_4OH , 100 °C (38%, two steps); (d) 5% Pd/dba_3 , $dppf$, $Zn(CN)_2$, $Zn(OAc)_2$, Zn , DMF, 95 °C (91%); (e) 2-(2-bromo-ethyl)-1,3-dioxolane, NaH, DMF/DMSO, rt (61%); (f) 1 N HCl, acetone, 55 °C; (g) R_2NH , $Na(OAc)_3BH$, AcOH, CH_2Cl_2 (50–60%, two steps); (h) Raney-Ni, H_2 (30 psi), 2 M $NH_3/EtOH$; (i) benzoyl chloride or 4-fluorobenzoyl chloride, pyridine, CH_2Cl_2 (51–64%, two steps).

Table 1
SAR of 6-arylpyridazinone CatS inhibitors^a

Compound	NR_2	R'	CatS IC_{50} (μ M)
8		H	14
9		H	1.6
10 11		H F	2.3 1.5
12 13		H F	0.43 0.32

^a CatS IC_{50} values are the mean of $n \geq 2$ runs and determined as described previously.^{6a}

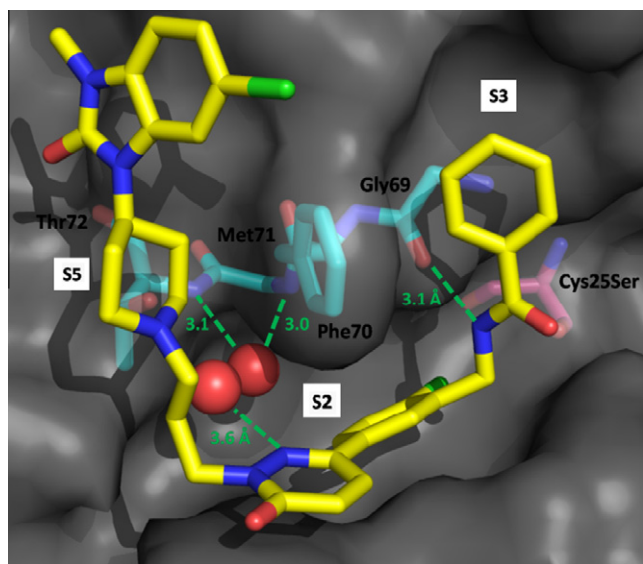


Figure 3. Crystal structure of pyridazinone **12** bound to Cys25Ser cathepsin S (PDB code: 3MPF). Two water molecules (red) are observed in the back of the S2 subsite. Hydrogen bonds are shown in green.

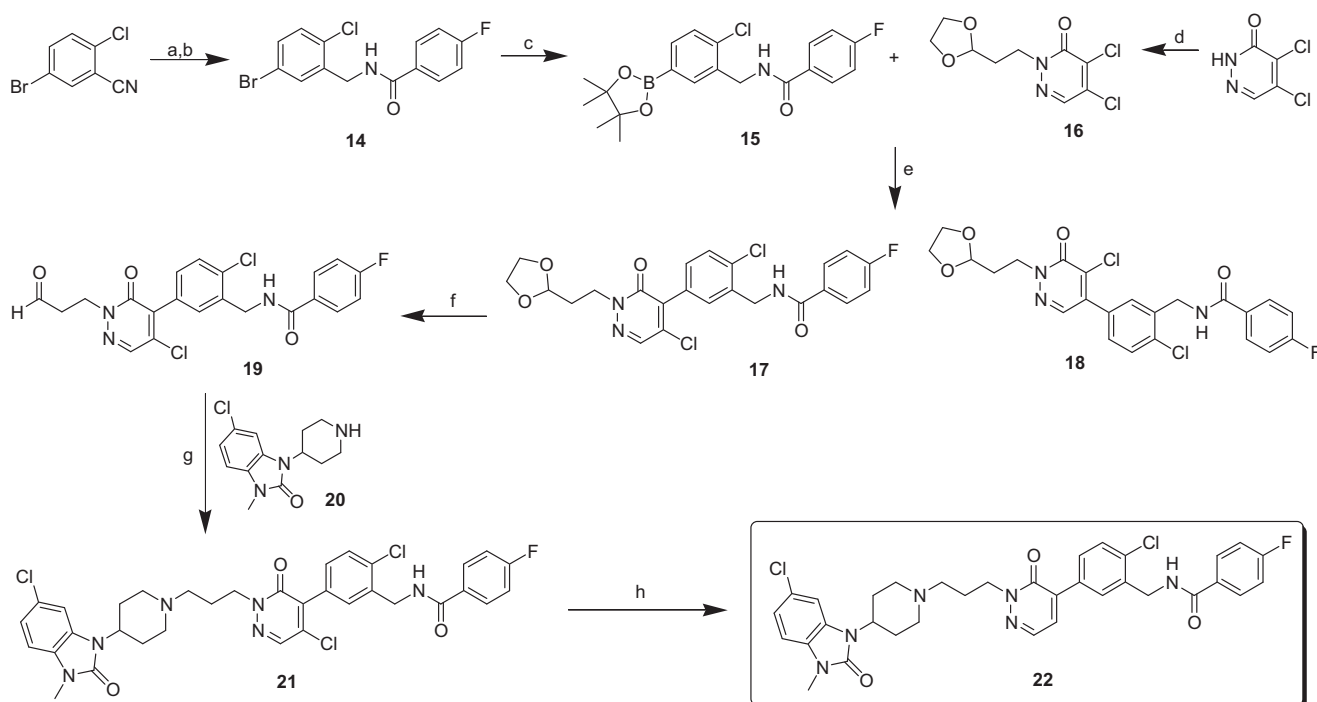
the nitrile to a primary amine while leaving the arylchloride and electron-poor pyridazinone ring intact. Furthermore, it was necessary to use ammonia in ethanol as a solvent for this reaction in order to suppress dimerization of the desired amine product. Based on previously established SAR for pyrazole-based CatS inhibitors, we surveyed several specific cyclic amines as P5 groups, and also focused on benzamide and 4-fluorobenzamide as P3 moieties.

As shown in Table 1, the enzymatic activity of compounds **8–13** varied dramatically with the nature of the P5 amine. Although pyrrolidine **8** displayed only mid-micromolar inhibition of CatS activ-

ity, piperazine **9** and piperidines **10–11** exhibited a six- to ninefold improvement in potency. The incorporation of a ketobenzimidazole-substituted piperidine yielded the most significant boost in activity, as evidenced by the sub-micromolar IC_{50} s for compounds **12** and **13**. The effect of the P3 amide on CatS inhibition was more subtle, with the 4-fluorobenzoyl group consistently providing a minimal improvement in potency over the parent benzamide (cf. **10** vs **11** and **12** vs **13**). Although the best inhibitor from this series, pyridazinone **13**, displayed only moderate enzymatic activity (hCatS IC_{50} = 320 nM), it is important to note that this constitutes more than a 500-fold improvement from the lead Tethering monophore **4**.

In order to glean insight into the binding mode of the 6-arylpyridazin-3-one series, a crystal structure of **12** bound to Cys25Ser CatS was obtained (Fig. 3). Gratifyingly, this compound binds in an orientation consistent with the molecular modeling predictions for Tethering hit **3**. The bicyclic arylpyridazinone core occupies the S2 pocket, while the ketobenzimidazole piperidine and benzamide groups reside in S5 and S3, respectively. Notably, a hydrogen bond is observed between the backbone carbonyl of Gly69 in S3 and the P3 benzamide N–H. However, the most intriguing contacts between the protein and inhibitor **12** occur within an area of S2 that spans Met71 and Thr72. In this region, two water molecules appear to facilitate a network of bridging interactions between N1 of the pyridazinone and the side chain hydroxyl group of Thr72, as well as the backbone amide hydrogens of Met71 and Thr72.

Since the pyridazinone ring in **12** binds only indirectly to the residues in S2, we anticipated that an alternate P2 group capable of displacing one or both of the water molecules would bind deeper in the S2 pocket and also benefit from the entropic gain associated with the release of these waters.¹⁷ The simplest analog of pyridazinone **12** that fits this description is the isomeric 4-arylpyridazin-3-one **22** (Scheme 2). This heterocycle retains the 1,3-disposition of the aromatic group and aminopropyl linker required to access S3 and S5, respectively. In addition, the polar carbonyl



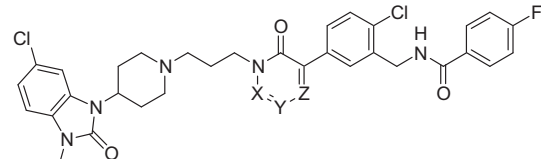
Scheme 2. Reagents and conditions: (a) BH_3 –THF, THF, rt; (b) 4-fluorobenzoyl chloride, pyr., CH_2Cl_2 (53%, two steps); (c) bis(pinacolato)diboron, KOAc, 10% $PdCl_2(dppf)$, DMF, 90 °C (87%); (d) 2-(2-bromoethyl)-1,3-dioxolane, CS_2CO_3 , DMF (69%); (e) 10% $PdCl_2(dppf)$, 2 M Na_2CO_3 /dioxane, 90 °C, (48%, **17**:**18** = 1:1.3); (f) 1 N HCl/acetone, 55 °C; (g) $Na(OAc)_3BH$, AcOH, CH_2Cl_2 (87%, two steps); (h) Et_3N , HCO_2H , $Pd(OAc)_2$, PPH_3 , DMF, 60 °C (98%).

group of the pyridazinone should be oriented directly towards the proximal water molecule situated in the back of the S2 pocket. Based on the SAR from Table 1, 4-fluorobenzamide was selected as a P3 group and incorporated into the key boronic ester intermediate **15**. The subsequent Suzuki coupling with dichloropyridazinone **16** proceeded unselectively to afford a separable mixture of arylpyridazinone isomers.¹⁸ The desired 4-aryl isomer **17** was ultimately joined with the ketobenzimidazole piperidine P5 group **20** to provide pyridazinone **22**.

In addition to pyridazinone **22**, we also prepared the diazinone isomers **27** (Scheme 3) and **32** (Scheme 4). These compounds possessed the structural features required for binding in S2, S3, and S5, and also allowed us to evaluate the importance of the position of the nitrogen atom within the diazine ring. Pyrimidinone **27** ultimately derived from bromopyrimidine **23**,¹⁹ boronic ester **15**, and ketobenzimidazole piperidine **20**. A similar series of synthetic transformations was used to assemble pyrazinone **32**, with chloropyrazine **28** functioning as the electrophile for the key Suzuki coupling.

As shown in Table 2, all three diazinone isomers demonstrated improved CatS inhibition relative to pyridazinone **13**, with pyrimidinone **27** exhibiting the most dramatic difference (hCatS IC₅₀ = 40 nM vs 320 nM for **13**). However, pyridazinone **22** displayed the best activity in a secondary cellular assay used to mea-

Table 2
SAR of diazinone-based CatS inhibitors^a

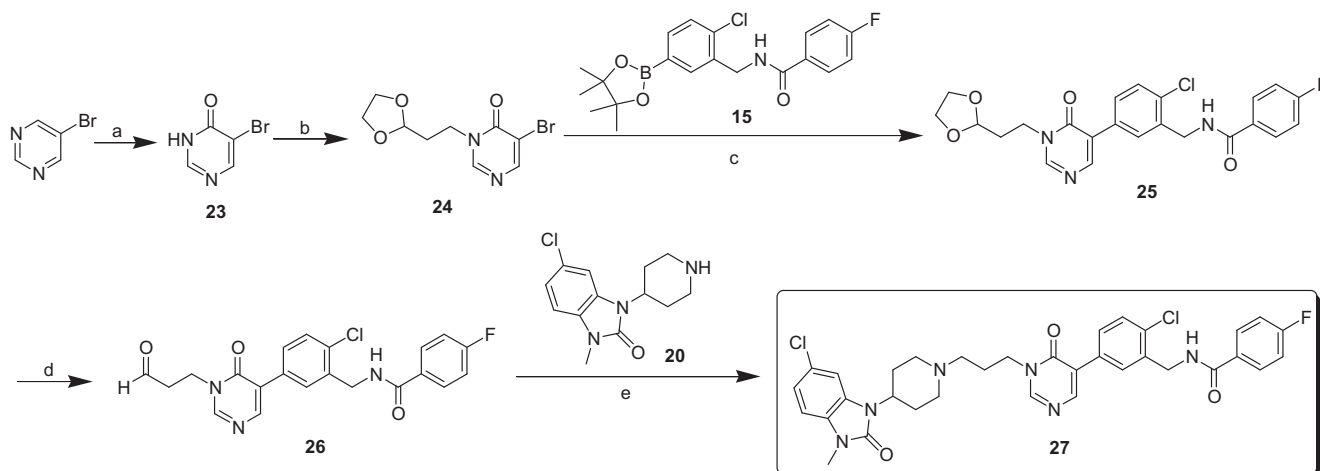


Compound	R	X	Y	Z	CatS IC ₅₀ (μM)	JY Li IC ₅₀ (μM)
22	H	N	CH	CH	0.06	1.8
27	H	CH	N	CH	0.04	6.7
32	H	CH	CH	N	0.11	8.0

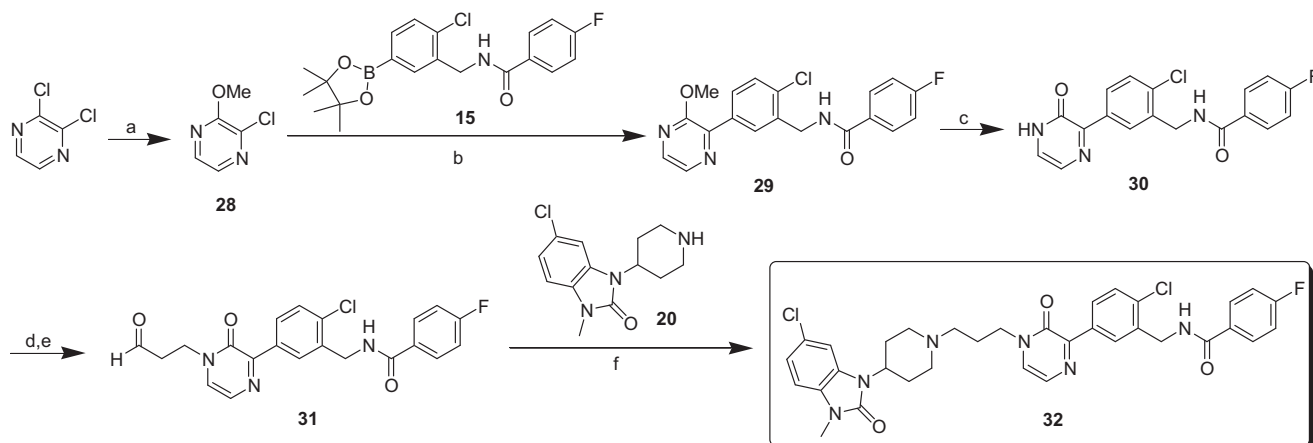
^a CatS IC₅₀ values and JY Li IC₅₀ values are the mean of $n \geq 2$ runs and determined as described previously.^{6a}

sure inhibition of invariant chain (Ii) degradation in a human B-cell line. In comparison, pyrimidinone **27** and pyrazinone **32** showed markedly reduced cellular activity, and these trends correlated only marginally well with cellular permeability.²⁰

In order to discern the structural factors responsible for the improved enzymatic activity of pyrimidinone **27**, we obtained a crystal structure of this compound bound to Cys25Ser CatS (Fig. 4). In



Scheme 3. Reagents and conditions: (a) H₃CO₃H, H₂SO₄, acetone (63%); (b) 2-(2-bromoethyl)-1,3-dioxolane, Cs₂CO₃, DMF (93%); (c) PdCl₂(dppf), K₃PO₄, dioxane, 90 °C (58%); (d) 1 N HCl, acetone, 55 °C; (e) Na(OAc)₃BH, AcOH, CH₂Cl₂ (53%, two steps).



Scheme 4. Reagents and conditions: (a) NaOMe, MeOH, 65 °C (71%); (b) PdCl₂(dppf), 2 M Na₂CO₃, dioxane, 90 °C; (c) 4 N HCl, 100 °C (48%, two steps); (d) 2-(2-bromoethyl)-1,3-dioxolane, Cs₂CO₃, DMF (87%); (e) 1 N HCl/acetone, 55 °C; (f) Na(OAc)₃BH, AcOH, CH₂Cl₂ (46%, two steps).

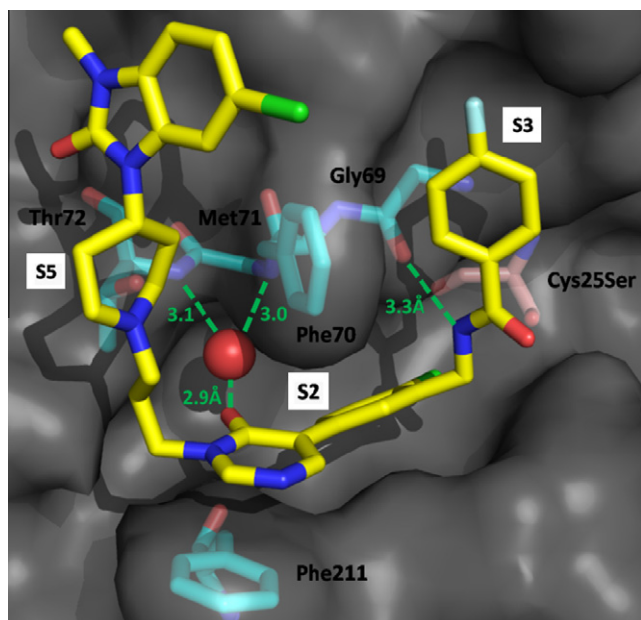


Figure 4. Crystal structure of pyrimidinone **27** bound to Cys25Ser cathepsin S (PDB code: 3MPE). A bridging water molecule (red) is observed in the back of the S2 subsite. Hydrogen bonds are shown in green.

general, the binding modes for pyrimidinone **27** and pyridazinone **12** (Fig. 3) are very similar, with both inhibitors spanning S3, S2, and S5 and interacting with the protein through only one direct hydrogen bond (Gly69). However, although a conserved water molecule is still present in the back of the S2 pocket for pyrimidinone **27**, it appears that the carbonyl group of the inhibitor did indeed displace the second water molecule observed in the crystal structure of pyridazinone **12**. Thus, it is possible that the eightfold improvement in activity for **27** relative to **12** can be attributed to several factors: (1) the entropic gain associated with the release of a bound water,¹⁷ (2) a stronger donor–acceptor interaction between the bound water and the pyrimidinone carbonyl (2.9 Å) compared to the pyridazinone nitrogen (3.6 Å), and (3) the fact that the water molecule bound to **27** interacts directly with the backbone amides of Met71 and Thr72, unlike the water molecule bound to **12** which can only interact with these residues through another bridging water. It is also important to note that pyridazinone **22**, pyrimidinone **27**, and pyrazinone **32** all show similar enzymatic activity, suggesting that the position of the second diazinone nitrogen atom is not essential. This may be attributed to the fact that these diazinones are all electron-poor heterocycles which appear to interact with the protein through a face-to-face π -stacking interaction with Phe211 in S2.

In conclusion, a pyridazin-4-one fragment **4** (hCatS = 170 μ M) discovered through Tethering was modeled into cathepsin S and predicted to overlap in S2 with the tetrahydropyridinepyrazole core of a previously disclosed series of CatS inhibitors. This fragment served as a template to design pyridazin-3-one **12** (hCatS = 430 nM), which also incorporates P3 and P5 binding elements. A crystal structure of **12** bound to Cys25Ser CatS revealed a pair of bound water molecules in the back of the S2 pocket that facilitate a network of bridging interactions between the inhibitor and the protein. The oxygen atom of pyrimidinone **27** (hCatS = 40 nM) is able to displace one of these bound waters, resulting in an eightfold improvement in enzymatic activity.

References and notes

- Roberts, R. *Drug News Perspect.* **2005**, *18*, 605.
- (a) Gupta, S.; Kumar Singh, R.; Dastidar, S.; Ray, A. *Exp. Opin. Ther. Targets* **2008**, *12*, 291; (b) Liu, W.; Spero, D. M. *Drug News Perspect.* **2004**, *17*, 357.
- Nakagawa, T. Y.; Brissette, W. H.; Lira, P. D.; Griffiths, R. J.; Petrushova, N.; Stock, J.; McNeish, J. D.; Eastman, S. E.; Howard, E. D.; Clarke, S. R. M.; Rosloniec, E. F.; Elliott, E. A.; Rudensky, A. *Immunity* **1999**, *10*, 207.
- (a) Burden, R. E.; Gormley, J. A.; Jaquin, T. J.; Small, D. M.; Quinn, D. J.; Hegarty, S. M.; Ward, C.; Walker, B.; Johnston, J. A.; Olwill, S. A.; Scott, C. J. *Clin. Cancer Res.* **2009**, *15*, 6042; (b) Taleb, S.; Clement, K. *Clin. Chem. Lab. Med.* **2007**, *45*, 328; (c) Lutgens, E.; Faber, B.; Schapira, K.; Evelo, C. T. A.; van Haften, R.; Heeneman, S.; Kitty, B. J. M.; Cleutjens, A. P. B.; Beckers, L.; Porter, J. G.; Mackay, C. R.; Rennert, P.; Bailly, V.; Jarpe, M.; Dolinski, B.; Kotliansky, V.; de Fougères, T.; Daeman, M. J. A. P. *Circulation* **2005**, *111*, 3443; (d) Wendt, W.; Lubbert, H.; Stichel, C. C. *Brain Res.* **2008**, *1232*, 7; (e) Irie, O.; Kosaka, T.; Ehara, T.; Yokokawa, F.; Kanazawa, T.; Hirao, H.; Iwasaki, A.; Skakai, J.; Teno, N.; Hitomi, Y.; Iwasaki, G.; Fukaya, H.; Nonomura, K.; Tanabe, K.; Koizumi, S.; Uchiyama, N.; Bevan, S. J.; Malcangio, M.; Gentry, C.; Fox, A. Y.; Yaqoob, M.; Culshaw, A. J.; Hallett, A. J. *Med. Chem.* **2008**, *51*, 5502.
- Thurmond, R. L.; Beavers, M. P.; Cai, H.; Meduna, S. P.; Gustin, D. L.; Sun, S.; Almond, H. J.; Karlsson, L.; Edwards, J. P. *J. Med. Chem.* **2004**, *47*, 4799.
- (a) Thurmond, R. L.; Sun, S.; Sehon, C. A.; Baker, S. M.; Cai, H.; Gu, Y.; Jiang, W.; Riley, J. P.; Williams, K. N.; Edwards, J. P.; Karlsson, L. J. *Pharmacol. Exp. Ther.* **2004**, *308*, 268; (b) Gustin, D. J.; Sehon, C. A.; Wei, J.; Cai, H.; Meduna, S. P.; Khatuya, H.; Sun, S.; Gu, Y.; Jiang, W.; Thurmond, R. L.; Karlsson, L.; Edwards, J. P. *Bioorg. Med. Chem. Lett.* **2005**, *15*, 1687.
- (a) Allen, D.; Ameriks, M. K.; Axe, F. U.; Burdett, M.; Cai, H.; Choong, I.; Edwards, James P.; Lew, W.; Meduna, S. P. *PCT Int. Appl. WO2008100635A1*, 2008; (b) Allen, D.; Ameriks, M. K.; Axe, F. U.; Burdett, M.; Cai, H.; Choong, I.; Edwards, J. P.; Lew, W.; Meduna, S. P. *PCT Int. Appl. WO2008100620A2*, 2008.
- For recent reviews on fragment-based drug discovery, see: (a) Congreve, M.; Chessari, G.; Tisi, D.; Woodhead, A. J. *J. Med. Chem.* **2008**, *51*, 3661; (b) Jahnke, W.; Erlanson, D. A., Eds. *Fragment-Based Approaches in Drug Discovery. In Methods and Principles in Medicinal Chemistry*, Mannhold, R., Kubinyi, H., Folkers, G., Eds.; 2006; Vol. 34, Wiley-VCH: Weinheim, Germany.
- Fragment-based screening has been utilized to identify CatS inhibitors: Wood, W. J.; Patterson, A. W.; Tsuruoka, H.; Jain, R. K.; Ellman, J. A. *J. Am. Chem. Soc.* **2005**, *127*, 15521.
- The term Tethering is a service mark of Sunesis Pharmaceuticals Inc. for its fragment-based drug discovery: (a) Oslob, J. D.; Erlanson, D. A. *Drug Discovery Today* **2004**, *3*, 143; (b) Erlanson, D. A.; Braisted, A. C.; Raphael, D. R.; Randal, M.; Stroud, R. M.; Gordon, E. M.; Wells, J. A. *Proc. Natl. Acad. Sci. U.S.A.* **2000**, *97*, 9367.
- Turkenburg, J. P.; Lamers, M. B. A. C.; Brzozowski, A. M.; Wright, L. M.; Hubbard, R. E.; Sturt, S. L.; Williams, D. H. *Acta Crystallogr., Sect. D: Biol. Crystallogr.* **2002**, *D58*, 451.
- CatS cysteine mutants were expressed in SF9 cells as histidine-tagged proteins. Following purification over a Ni-NTA column, the CatS mutants were processed by 0.4 mg/mL pepsin, 100 mM NaOAc, pH 4.5, 5 mM DTT, 2.5 mM EDTA for 2 h at 40 °C. Pepsin enzymatic activity was stopped by raising the pH of the digestion to 7.5. Further purification was not required for screening, since the molecular weight of pepsin is larger than CatS and does not interfere with deconvolution of the fragment hits.
- Monophore screening conditions: 10–15 μ M CatS mutant, 1 mM β -mercaptoethanol, 50 μ M monophore (500 μ M total in pools of 10), 50 mM Tris, pH 7.5. Monophore hits were identified by visual inspection of the deconvoluted masses of the monophore-protein conjugates and then ranked by fractional conjugation (the fraction of protein that remains conjugated to the discrete monophores in the presence of increasing concentrations of β -mercaptoethanol).
- For a detailed description of the enzymatic assay, see: Allen, D.; Choong, I.; Lew, W. *PCT Int. Appl. WO2008100622A2*, 2008.
- The monophore corresponding to adduct **3** was non-covalently docked to the structure of CatS in the area surrounding the E115C residue. Only binding conformations that placed the sulfur of the linker within 5 Å of the cysteine residue were retained. The monophores were then covalently attached as disulfides to the cysteine mutant and minimization was attempted to match each conformation from the non-covalent docking. The conformations were then scored and the lowest energy conformation for adduct **3** is shown in Figure 2.
- Coates, W. J.; McKillop, A. *Synthesis* **1993**, *25*, 334.
- (a) Barillari, C.; Taylor, J.; Essex, J. W. *J. Am. Chem. Soc.* **2007**, *129*, 2577; (b) Lu, Y.; Chao-Yie, Y.; Wang, S. J. *Chem. Inf. Model.* **2007**, *47*, 668; (c) Hamelberg, D.; McCammon, J. A. *J. Am. Chem. Soc.* **2004**, *126*, 7683.
- Gong, Y.; He, W. *Heterocycles* **2004**, *62*, 851.
- Kress, T. J. *J. Org. Chem.* **1985**, *50*, 3073.
- TC7 cellular permeability data (Cerep, Inc.), P_{app} (10^{-6} cm/s): compound **22**, A–B = 1.3/B–A = 1.5; compound **27**, A–B = 2.5/B–A = 2.9; compound **32**, A–B = 0.6/B–A = 3.7.